Available online at www.sciencedirect.com
SCIENCE DIRECT®
Journal of Sound and Vibration 290 (2006) 882–909
JOURNAL OF SOUND AND VIBRATION
www.elsevier.com/locate/jsvi

On the modelling of excitations in geared systems by transmission errors

P. Velex*, M. Ajmi

LaMCoS—UMR CNRS 5514, Bâtiment Jean d'Alembert, INSA de Lyon, 20, Avenue Albert Einstein, 69 621 Villeurbanne Cedex, France

Received 26 February 2004; received in revised form 21 February 2005; accepted 29 April 2005
Available online 24 August 2005

Abstract

This paper introduces an original theoretical approach to the modelling of pinion–gear excitations valid for three-dimensional models of single-stage geared transmissions. Shape deviations and errors on gears are considered and the associated equations of motion account for time-varying mesh stiffness, and also torsional, flexural and axial couplings. Starting from the instantaneous contact conditions between the teeth, the equations of motion are re-formulated in terms of quasi-static transmission errors under load and no-load transmission errors. The range of application of transmission error-based formulations is analysed and some new equations are proposed which make it possible to introduce rigorously meshing excitations via transmission errors. Using an extended finite element model of a spur and helical gear test rig, the dynamic results from the formulations based on transmission errors are compared with the reference solutions. Both sets of results are found to be in close agreement, thus validating the proposed theory. The paper concludes with a critical analysis of the interests and limitations concerning the concept of transmission errors as excitation terms in gear dynamics.

1. Introduction

Over recent decades, many attempts have been made by numerous authors to set up models aimed at simulating the dynamic behaviour of gears [1–5]. The mathematical formulations range

*Corresponding author. Tel.: +33 472 438457; fax: +33 478 890980.
E-mail address: Philippe.Velex@insa-lyon.fr (P. Velex).

0022-460X/$ - see front matter © 2005 Elsevier Ltd. All rights reserved.
doi:10.1016/j.jsv.2005.04.033

Nomenclature

C_m	input torque on pinion shaft
C_{m0}	nominal resisting torque ($=(Rb_1/Rb_2)C_r$)
C_r	output torque on gear shaft
$\mathbf{C}_v$	$\bar{\mathbf{K}}^{-1}\mathbf{V}$
C_{wv}	$\mathbf{W}^{\mathrm{T}}\bar{\mathbf{K}}^{-1}\mathbf{V}$
C_{vv}	$\mathbf{V}^{\mathrm{T}}\bar{\mathbf{K}}^{-1}\mathbf{V}$
e_k	eccentricity on solid k
$\mathbf{E}(\vartheta)$	see Eq. (14)
F_t	tangential static mesh force ($=C_{m0}/Rb_1=C_r/Rb_2$)
F_d	dynamic normal mesh force
F_{s}	static normal mesh force
$\mathbf{F}(\vartheta)$	see Eq. (14)
$\mathbf{F}_0$	constant force vector
$g(\vartheta)$	shape function of mesh stiffness
$\mathbf{G}(\vartheta)$	see Eq. (14)
I_1, I_2	transverse moment of inertia of pinion, of gear
I_{p1}, I_{p2}	polar moment of inertia of pinion, of gear
J_1, J_2	polar moment of inertia of the pinion, of the gear shaft line
K	subscript (1 corresponds to pinion, 2 to gear)
k_i	mesh stiffness associated with the ith discretization cell of contact lines
k_m	average mesh stiffness
$\mathbf{K}$	stiffness matrix with the contributions of pinion and gear excluded
$\bar{\mathbf{K}}$	averaged total stiffness matrix
m_k	mass of solid k
m_{eq}	equivalent mass ($=J_1J_2/(J_1\mathrm{Rb}_2^2+J_2\mathrm{Rb}_1^2)$)
M_i	ith potential point of contact on contact lines
$\mathbf{M}$	total mass matrix
$\mathbf{n}_1$	outer unit normal vector to pinion tooth flanks
$N(t)$	time-varying number of contacting cells
NLTE	no-load transmission error
O_1, O_2	centre of pinion, of gear
$\mathrm{Rb}_1, \mathrm{Rb}_2$	base radius of pinion, of gear
t	time
Tm	mesh period
T'_1, T'_2	limits of meshing area on base plane
TE	transmission error under load
TE_s	quasi-static transmission error under load
u_k	axial elastic displacement of solid k
$\mathbf{u}_k^R(\mathbf{O}_k)$	translational displacement vector of solid k in O_k with respect to rigid-body motions
U	total strain energy
U_g	pinion–gear strain energy
v_k	elastic displacement of solid k in the radial direction $(O_k, \vec{s})$
v_x	$\mathbf{V}^{\mathrm{T}}\mathbf{X}$
v_{xs}	$\mathbf{V}^{\mathrm{T}}\mathbf{X}_s$
v_{xD}	$\mathbf{V}^{\mathrm{T}}\mathbf{X}_D$
$\underset{\sim}{v}_{x0}$	$\mathbf{V}^{\mathrm{T}}\underset{\sim}{\mathbf{X}}_0$
$\widetilde{v}_{x0}$	$\mathbf{V}^{\mathrm{T}}\mathbf{X}_0$
$\mathbf{V}, \mathbf{V}(\mathbf{M}_i)$	averaged, actual structure vector at M_i
w_k	elastic displacement of solid k in the radial direction $(O_k, \vec{t})$
w_{x0}	$\mathbf{W}^{\mathrm{T}}\underset{\sim}{\mathbf{X}}_0$
$\widetilde{w}_{x0}$	$\mathbf{W}^{\mathrm{T}}\mathbf{X}_0$
x	$\mathrm{Rb}_1\theta_1+\mathrm{Rb}_2\theta_2$
$x_D, \mathbf{X}_D$	dynamic component of x, of $\mathbf{X}$
$x_S, \mathbf{X}_S$	quasi-static component of x, of $\mathbf{X}$
$\mathbf{X}$	elastic displacement vector
α	amplitude ratio in the expression of the mesh stiffness function ($\alpha \prec 1$)
β, β_b	helix, base helix angle
$\delta(M_i)$	deflection at a potential point of contact M_i
$\delta e(M_i)$	equivalent normal deviation at a potential point of contact M_i
λ_k	phase of eccentricity of solid k
ϕ_1, ϕ_2	angular degree of freedom (dof) of pinion, of gear about $\vec{s}$
ψ_1, ψ_2	angular dof of pinion, of gear about $\vec{t}$
θ_1, θ_2	torsional dof of pinion, of gear
$\boldsymbol{\omega}_k^R$	angular displacement vector of solid k with respect to rigid-body motions
$\vartheta=\Omega_1 t$	angular variable
Ω_1, Ω_2	rigid-body angular velocity of pinion, of gear

Symbols

$\dot{A}$ time derivative of A

A' derivative of A with respect to $\vartheta = \Omega_1 t$

$\tilde{\mathbf{A}}$ restriction of $\mathbf{A}$ to the pinion–gear dof

$\mathbf{A}^{\mathrm{T}}$ $\mathbf{A}^{\mathrm{T}}$: transpose of $\mathbf{A}$

$\mathbf{A}$ column vector or matrix

from single-degree-of freedom (sdof) models to finite element three-dimensional (3D) ones, but virtually all gear dynamic models consider that transmission error and variations in mesh stiffness are the primary sources of excitation. From the gear designer's point of view, the definition of tooth modifications for low-noise gears also relies on the minimization of transmission error variations [6–8]. However, most of the theoretical background stems from sdof torsional models [9] and very little attention has been given to the validity and limits of the concept of transmission errors as excitation sources, particularly in the case of multi-degree-of-freedom (mdof) 3D systems. Rather than developing a new mathematical model, some existing theoretical works are investigated in the present paper with the objective of clarifying the role of transmission errors as excitations in gear dynamics. Firstly, the classical sdof torsional model is re-examined in order to provide a detailed analysis of the links between no-load, under load, quasi-static transmission errors and forcing terms. Next, the analysis is extended to 3D mdof systems and a sound theoretical background is derived for excitation modelling based on transmission errors. To this end, the excitations associated with tooth meshing are derived from the instantaneous contact conditions between mating tooth flanks and not from prior quasi-static analyses as is the case in the vast majority of the models found in the literature. The connections with transmission errors are then examined from a theoretical point of view and commented upon. All developments are conducted from models of single-stage geared systems which account for time-varying mesh stiffness, gear errors and tooth shape modifications.

2. Generalities

2.1. State of reference—rigid-body motions

Rigid-body rotations represent the state of reference [10] characterized by the following kinematic and dynamic equations. At all non-singular points of contact M^* between the pinion and gear, rigid-body kinematics implies that (off-line-of-action contacts not being considered)

$$\mathbf{V}_2^1(\mathbf{M}^*) \cdot \mathbf{n}_{M^*} = 0 \tag{1}$$

with $\mathbf{n}_{M^*}$, a unit normal vector at M^* which, when introducing the time-derivative of no-load (or rigid-body) transmission error NLTE projected as a distance on the base plane, is equivalent to

$$\frac{\mathrm{d}}{\mathrm{d}t}(\mathrm{NLTE}) = \mathrm{Rb}_1\,\Omega_1 + \mathrm{Rb}_2\,\Omega_2, \tag{2}$$

where Rb_1, Rb_2 are the base radii of the pinion and the gear, and Ω_1, Ω_2 are the rigid-body angular velocity of the pinion and gear, respectively.

Using the Kinetic Energy Theorem, the rigid-body dynamic behaviour for frictionless gears is controlled by

$$J_1\Omega_1\dot{\Omega}_1 + J_2\Omega_2\dot{\Omega}_2 = C_m\Omega_1 + C_r\Omega_2 \tag{3}$$

with J_1, J_2 being the polar moments of inertia of the pinion shaft line and the gear shaft line, respectively, and C_m, C_r are the pinion and gear torques.

The system with 4 unknowns (Ω_1, Ω_2, C_m, C_r) is characterized by Eqs. (2) and (3) only, and 2 parameters have to be imposed. In the rest of the text, the pinion speed Ω_1 and the output torque C_r are supposed to be known and constant. In these conditions, the kinematic and dynamic unknowns are deduced as

$$\Omega_2 = -\frac{\mathrm{Rb}_1}{\mathrm{Rb}_2}\Omega_1 + \frac{1}{\mathrm{Rb}_2}\frac{\mathrm{d}}{\mathrm{d}t}(\mathrm{NLTE}), \tag{4}$$

$$C_m \cong \frac{\mathrm{Rb}_1}{\mathrm{Rb}_2}\left[C_r - \frac{J_2}{\mathrm{Rb}_2}\frac{\mathrm{d}^2}{\mathrm{d}t^2}(\mathrm{NLTE})\right] \cong C_{m0} - \frac{J_2}{\mathrm{Rb}_2^2}\mathrm{Rb}_1\frac{\mathrm{d}^2}{\mathrm{d}t^2}(\mathrm{NLTE}), \tag{5}$$

where $C_{m0} = (\mathrm{Rb}_1/\mathrm{Rb}_2)C_r$ is the nominal resisting torque, i.e., in the absence of no-load transmission error.

2.2. Deformed state

2.2.1. Contact deflection

For any discrete model with two nodes at the pinion and gear centers, respectively, and a maximum of 6 degrees of freedom (dof) per node, the pinion–gear pair can be assimilated to two rigid cylinders linked by a time-varying set of lumped stiffnesses along the potential lines of contact on the base plane (Fig. 1). In such conditions, elastic displacements can be described by screws $\{D_k\}$ associated with the pinion and gear of the form

$$\{D_k\}\begin{Bmatrix}\boldsymbol{\omega}_k^R \\ \mathbf{u}_k^R(\mathbf{O}_k)\end{Bmatrix}, \tag{6a}$$

where $k = 1$ for the pinion and $k = 2$ for the gear, $\boldsymbol{\omega}_k^R$ is the angular displacement vector and $\mathbf{u}_k^R(\mathbf{O}_k)$ is the translational displacement vector at the pinion and gear centres.

In the particular case of torsional models, the displacement screws reduce to

$$\{D_k\}\begin{Bmatrix}\theta_k\mathbf{z} \\ \mathbf{0}\end{Bmatrix}. \tag{6b}$$

The deflection at any potential point of contact M_i (i.e., the normal approach relative to rigid-body motions minus the initial gap due to errors and/or shape modifications) can be expressed as

$$\begin{aligned}\delta(M_i) &= \sum_{k=1}^{2}\left(\mathbf{u}_k^R(\mathbf{O}_k) + \boldsymbol{\omega}_k^R \times \mathbf{O}_k\mathbf{M}_i\right)\cdot\mathbf{n}_k - \delta e(M_i) \\ &= \mathbf{V}(\mathbf{M}_i)^{\mathrm{T}}\mathbf{X} - \delta e(M_i),\end{aligned} \tag{7}$$

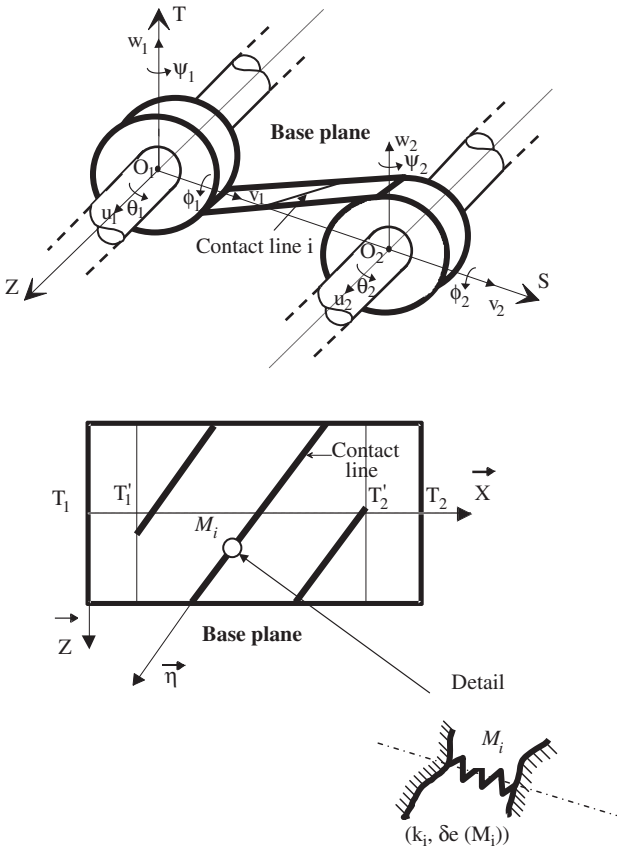

Fig. 1. Gear Model (12 dof), mesh elasticity and shape deviation modelling.

where $\delta e(M_i)$ is the difference between the maximum of $e(M_i)$ and $e(M_i)$ at time t, $e(M_i)$ is the normal composite deviation (pinion + gear) at M_i. $\mathbf{X}$ is the total dof vector. $\mathbf{V}(\mathbf{M}_i)$, the structure vector [11,12], accounts for the particular gear geometry, and its restriction to the pinion–gear dof is (the other components being zero)

$$\tilde{\mathbf{V}}(\mathbf{M}_i)^{\mathrm{T}} = (\mathbf{n}_1, \mathbf{O}_1\mathbf{M}_i \times \mathbf{n}_1, -\mathbf{n}_1, -\mathbf{O}_2\mathbf{M}_i \times \mathbf{n}_1). \tag{8a}$$

In the particular case of torsional models, the non-zero components of the structure vector are

$$\tilde{\mathbf{V}}(\mathbf{M}_i)^{\mathrm{T}} = \cos\beta_b \langle \mathrm{Rb}_1, \mathrm{Rb}_2 \rangle. \tag{8b}$$

2.2.2. Transmission error under load

According to Harris [13], Munro [14], etc., transmission error (TE) is a measure of departure from perfect motion transfer between the pinion and gear where 'perfect' refers to perfectly mounted rigid bodies with ideal geometries. The definition of transmission error under load is clear when using the classical sdof torsional model since it relates directly to the angles of torsion

of the pinion and gear. For other models (even purely torsional ones), the definition of TE is ambiguous or at least not intrinsic. This is because its value can vary depending on the chosen nodes (or cross-sections) of reference for measuring or calculating deviations between actual and perfect rotation transfers from the pinion to the gear [15]. Throughout this paper, transmission error is defined by extrapolating the usual experimental practice based on encoders or accelerometers, i.e., from the actual total angles of rotation, either measured or calculated at one section of reference on the pinion shaft (subscript I) and on the gear shaft (subscript II) as schematically represented in Fig. 3. After projection on the theoretical base plane, one obtains

$$\mathrm{TE} = \mathrm{Rb}_1\left[\int_0^t \Omega_1\,\mathrm{d}\zeta + \theta_\mathrm{I}\right] + \mathrm{Rb}_2\left[\int_0^t \Omega_1\,\mathrm{d}\zeta + \theta_\mathrm{II}\right] = \mathrm{Rb}_1\theta_\mathrm{I} + \mathrm{Rb}_2\theta_\mathrm{II} + \mathrm{NLTE} \tag{9}$$

with ζ, a dummy integration variable and θ_I, θ_II, the torsional perturbations with respect to rigid-body rotations (dof) at node I on the pinion shaft and at node II on the gear shaft.

Introducing a projection vector $\mathbf{W}$ of components Rb_1 and Rb_2 at the positions corresponding to the torsional dof at nodes I and II and with zeros elsewhere, transmission error under load can finally be expressed as

$$\mathrm{TE} = \mathbf{W}^\mathrm{T}\mathbf{X} + \mathrm{NLTE}. \tag{10}$$

2.2.3. Equations of motion

Based on the gear mesh interface model in Fig. 1, the gear strain energy is

$$U_g = \frac{1}{2}\sum_i^{N(t)} k_i\delta(M_i)^2 = \frac{1}{2}\mathbf{X}^\mathrm{T}\sum_i^{N(t)} k_i\mathbf{V}(\mathbf{M}_i)\mathbf{V}(\mathbf{M}_i)^\mathrm{T}\mathbf{X} - \mathbf{X}^\mathrm{T}\sum_i^{N(t)} k_i\delta e(M_i)\mathbf{V}(\mathbf{M}_i) + \frac{1}{2}\sum_i^{N(t)} k_i\delta e(M_i)^2 \tag{11}$$

with $N(t)$ being the instantaneous number of active (loaded) stiffnesses at time t.

In the case of linear elements for shafts, bearings, couplings, etc., the total strain energy reads

$$U = U_g + \tfrac{1}{2}X^\mathrm{T}\mathbf{K}\mathbf{X}, \tag{12}$$

where $\mathbf{K}$ is a constant stiffness matrix which accounts for everything except the pinion and the gear.

Neglecting both second-order terms and gyroscopic components, the kinetic energy relative to the inertial frame of a pinion–gear pair becomes [10]

$$T_g = \frac{1}{2}\sum_{k=1}^{2} m_k\left[\dot{u}_k^2 + (\dot{v}_k + C_{sk})^2 + (\dot{w}_k + C_{tk})^2\right] + I_k\left[\dot{\phi}_k^2 + \dot{\psi}_k^2\right] + I_{pk}\left[\Omega_k + \dot{\theta}_k\right]^2 \tag{13}$$

with $C_{sk} \cong -e_k\Omega_k\sin(\Omega_k t - \lambda_k)$ and $C_{tk} \cong e_k\Omega_k\cos(\Omega_k t - \lambda_k)$, the consequences of possible eccentricities e_k on the pinion and/or the gear. m_k is the mass, I_k the transverse moment of inertia and I_{pk} the polar moment of inertia of the pinion or gear.

After applying Lagrange equations and replacing the time variable t with the angular variable $\vartheta = \Omega_1 t$, the equations of motions for the undamped system are derived under the form

$$\Omega_1^2 \mathbf{M}\mathbf{X}'' + \left[\mathbf{K} + \sum_i k_i \mathbf{V}(\mathbf{M}_i)\mathbf{V}(\mathbf{M}_i)^{\mathrm{T}}\right]\mathbf{X} = \mathbf{F}_0 + \sum_i k_i \delta e(M_i)\mathbf{V}(\mathbf{M}_i) - \Omega_1^2[\mathrm{NLTE}''\mathbf{E}(\vartheta) + \mathrm{NLTE}'\mathbf{F}(\vartheta) + \mathbf{G}(\vartheta)] \quad (14)$$

where $\mathbf{M}$ is the total mass matrix, $\mathbf{F}_0$ the constant force vector (nominal torques),

$$\tilde{\mathbf{E}}(\vartheta)^{\mathrm{T}} = \left(0,0,0,0,0,0,0,0,-m_2\frac{e_2}{\mathrm{Rb}_2}\sin(\Omega_2 t-\lambda_2), m_2\frac{e_2}{\mathrm{Rb}_2}\cos(\Omega_2 t-\lambda_2),0,0,\frac{I_{p2}}{\mathrm{Rb}_2}\right).$$

Apart from the components of $\tilde{\mathbf{E}}(\vartheta)$, the total vector $\mathbf{E}(\vartheta)$ comprises the following:

(i) $J_2\mathrm{Rb}_1/\mathrm{Rb}_2^2$ at the torsional dof associated with the input torque (from Eq. (5)),
(ii) I_{pi}/Rb_2 at all the torsional dof of the gear shaft as a consequence of the non-steady rotational speed when no-load transmission error is not nil (I_{pi} is the polar moment of inertia attached to node i).

$$\tilde{\mathbf{F}}(\vartheta)^{\mathrm{T}} = \left(0,0,0,0,0,0,0,0,2m_2\frac{e_2}{\mathrm{Rb}_2}\frac{\mathrm{Rb}_1}{\mathrm{Rb}_2}\cos(\Omega_2 t-\lambda_2), 2m_2\frac{e_2}{\mathrm{Rb}_2}\frac{\mathrm{Rb}_1}{\mathrm{Rb}_2}\sin(\Omega_2 t-\lambda_2),0,0,0\right),$$

$$\tilde{\mathbf{G}}(\vartheta)^{\mathrm{T}} = (0,-m_1e_1\cos(\Omega_1 t-\lambda_1),-m_1e_1\sin(\Omega_1 t-\lambda_1),0,0,0,0, -m_2e_2\left(\frac{\mathrm{Rb}_1}{\mathrm{Rb}_2}\right)^2\cos(\Omega_2 t-\lambda_2), -m_2e_2\left(\frac{\mathrm{Rb}_1}{\mathrm{Rb}_2}\right)^2\sin(\Omega_2 t-\lambda_2),0,0,0),$$

$$a' = \frac{\mathrm{d}}{\mathrm{d}\vartheta}a.$$

3. Sdof torsional models

In the interest of clarity, the analysis of transmission errors as excitation terms is first conducted by using the classical torsional model shown in Fig. 2, in order to privilege the methodological approach as opposed to the mathematical manipulations required by a 3D model. In such conditions, the differential system (14) reduces to

$$\Omega_1^2\begin{bmatrix}J_1 & 0\\ 0 & J_2\end{bmatrix}\begin{bmatrix}\theta_1''\\ \theta_2''\end{bmatrix} + \left(\sum_i k_i\right)\cos^2\beta_b\begin{bmatrix}\mathrm{Rb}_1^2 & \mathrm{Rb}_1\mathrm{Rb}_2\\ \mathrm{Rb}_1\mathrm{Rb}_2 & \mathrm{Rb}_2^2\end{bmatrix}\begin{bmatrix}\theta_1\\ \theta_2\end{bmatrix} = \begin{bmatrix}Cm_0\\ Cr\end{bmatrix} - J_2\frac{\mathrm{Rb}_1}{\mathrm{Rb}_2^2}\Omega_1^2\,\mathrm{NLTE}''\begin{bmatrix}1\\0\end{bmatrix} - \frac{J_2}{\mathrm{Rb}_2}\Omega_1^2\,\mathrm{NLTE}''\begin{bmatrix}0\\1\end{bmatrix} + \left(\sum_i k_i\delta e(M_i)\right)\cos\beta_b\begin{bmatrix}\mathrm{Rb}_1\\ \mathrm{Rb}_2\end{bmatrix}. \quad (15)$$

After multiplying the first line in Eq. (15) by Rb_1J_2, the second line by Rb_2J_1, adding the two equations and dividing all terms by $(J_1\mathrm{Rb}_2^2+J_2\mathrm{Rb}_1^2)$, the semi-definite system (15) is transformed

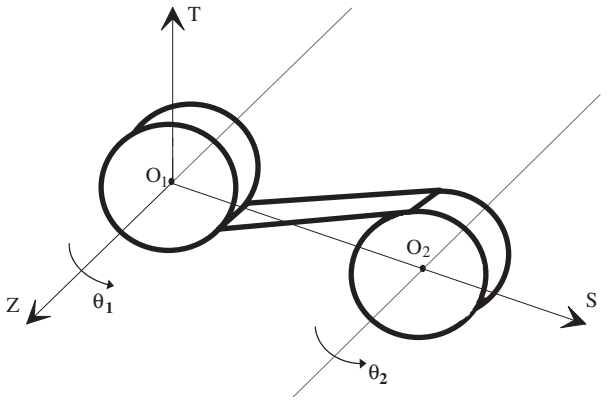

Fig. 2. Basic torsional model.

into the differential equation

$$\Omega_1^2 m_{\mathrm{eq}} x'' + \left(\sum_i k_i\right)\cos^2\beta_b x = \mathrm{Ft} + \left(\sum_i k_i \delta e(M_i)\right)\cos\beta_b - \Omega_1^2 \frac{J_2}{\mathrm{Rb}_2^2}\mathrm{NLTE}'' \tag{16}$$

where

$$x = \mathrm{Rb}_1\theta_1 + \mathrm{Rb}_2\theta_2,$$

$$m_{\mathrm{eq}} = \frac{J_1 J_2}{J_1\mathrm{Rb}_2^2 + J_2\mathrm{Rb}_1^2}, \quad \text{equivalent mass,}$$

$$\mathrm{Ft} = \frac{Cm_0}{\mathrm{Rb}_1} = \frac{Cr}{\mathrm{Rb}_2}, \quad \text{tangential static mesh force.}$$

The quasi-static equation is derived by imposing $\Omega_1 \to 0$ and reads

$$\left(\sum_i k_i\right)^S \cos^2\beta_b x_S = \mathrm{Ft} + \left(\sum_i k_i \delta e(M_i)\right)^S \cos\beta_b, \tag{17}$$

where superscript S refers to quasi-static values of the functions.

Assuming that the dynamic contact conditions are similar to the quasi-static ones (partial or total contact losses between the teeth and nonlinear jumps being excluded), so that

$$\left(\sum_i k_i\right)^S \cong \left(\sum_i k_i\right), \tag{18a}$$

$$\left(\sum_i k_i \delta e(M_i)\right)^S \cong \left(\sum_i k_i \delta e(M_i)\right), \tag{18b}$$

the dynamic equation can be re-written after separating the average and time-varying components of the mesh stiffness as

$$\Omega_1^2 m_{eq} x'' + k_m \cos^2\beta_b (1+\alpha g(\vartheta)) x = k_m \cos^2\beta_b (1+\alpha g(\vartheta)) x_S - \Omega_1^2 \frac{J_2}{\mathrm{Rb}_2^2} \mathrm{NLTE}'', \tag{19}$$

where k_m is the average mesh stiffness such that $\left(\sum_i k_i\right) = k_m(1+\alpha g(\vartheta))$ and $\alpha \prec 1$.

From the definition of transmission error under load in the direction of the line of action in Eq. (10), the equation of motion can be written in terms of the quasi-static transmission error under load TE_S and the no-load transmission error NLTE as

$$\begin{aligned}\Omega_1^2 m_{\mathrm{eq}} x'' + k_m \cos^2\beta_b (1+\alpha g(\vartheta)) x = {} & k_m \cos^2\beta_b (1+\alpha g(\vartheta))[\mathrm{TE}_s - \mathrm{NLTE}] \\ & - \Omega_1^2 \frac{J_2}{\mathrm{Rb}_2^2} \mathrm{NLTE}''.\end{aligned} \tag{20}$$

When considering the dynamic displacement $x_D = x - x_S$ as the major unknown, an alternative form of interest is derived as:

$$\Omega_1^2 m_{\mathrm{eq}} x_D'' + k_m \cos^2\beta_b (1+\alpha g(\vartheta)) x_D = -m_{\mathrm{eq}} \Omega_1^2 \left[\mathrm{TE}_S'' + \frac{J_2}{J_1} \frac{\mathrm{Rb}_1^2}{\mathrm{Rb}_2^2} \mathrm{NLTE}'' \right]. \tag{21}$$

The gear dynamic behaviour can be assessed by evaluating the corresponding dynamic tooth loading. To this end, the total instantaneous mesh force is introduced and determined by adding the forces in all the individual mesh stiffnesses on the base plane at a given time t as

$$F_D = \sum_i k_i \left[x \cos\beta_b - \delta e_i \right] = k_m (1+\alpha g(\vartheta)) \cos\beta_b x - \left(\sum_i k_i \delta e_i \right). \tag{22}$$

The static Eq. (17) leads to

$$\sum_i k_i \delta e_i = k_m (1+\alpha g(\vartheta)) \cos\beta_b x_S - F_S \tag{23}$$

with $F_S = \mathrm{Ft}/\cos\beta_b$, the static normal mesh force, and the dynamic mesh force is finally deduced as

$$F_D = F_S + k_m (1+\alpha g(\vartheta)) \cos\beta_b x_D. \tag{24}$$

4. 3D models of geared systems

4.1. Equations of motion

Following the same procedure as for the sdof model, the set of quasi-static equations associated with the equations of motion (14) is

$$\left[\mathbf{K} + \left(\sum_i k_i \mathbf{V}(\mathbf{M}_i) \mathbf{V}(\mathbf{M}_i)^{\mathrm{T}} \right)^S \right] \mathbf{X}_S = \mathbf{F}_0 + \left(\sum_i k_i \delta e(M_i) \mathbf{V}(\mathbf{M}_i) \right)^S, \tag{25}$$

Assuming that the instantaneous meshing conditions are independent of speed and remain close to those in quasi-static conditions, the equations of motion can be expressed as

$$\Omega_1^2\mathbf{M}\mathbf{X}'' + \left[\mathbf{K} + \left(\sum_i k_i\mathbf{V}(\mathbf{M}_i)\mathbf{V}(\mathbf{M}_i)^{\mathrm{T}}\right)\right]\mathbf{X} = \left[\mathbf{K} + \left(\sum_i k_i\mathbf{V}(\mathbf{M}_i)\mathbf{V}(\mathbf{M}_i)^{\mathrm{T}}\right)\right]\mathbf{X}_S - \Omega_1^2[\mathrm{NLTE}''\,\mathbf{E}(\vartheta) + \mathrm{NLTE}'\,\mathbf{F}(\vartheta) + \mathbf{G}(\vartheta)]. \quad (26)$$

4.2. Expression of the quasi-static deflection vector in terms of transmission errors

Contrary to the sdof model, the introduction of the quasi-static transmission error under load is not direct because Eq. (10) does not provide a one-to-one correspondence between TE_S and the static deflection vector $\mathbf{X}_S$. This difficulty can be resolved when replacing the actual structure vector $\mathbf{V}(\mathbf{M}_i)$ by its average value over one mesh period, denoted henceforth as $\mathbf{V}$ and independent of the position of the potential point of contact under consideration. This simplification is used (often implicitly) in the vast majority of the gear models in the literature and it slightly modifies the gear–pinion angular bending stiffnesses (with respect to ψ_1, ψ_2, ϕ_1 and ϕ_2 according to the terminology in Fig. 3) which are of secondary importance for narrow-faced gears. In such conditions, the static equations can be re-written as

$$\bar{\mathbf{K}}\mathbf{X}_S = \mathbf{F}_0 + \left(\sum_i k_i\delta e(M_i)\right)\mathbf{V} - \alpha k_m g(\vartheta)\mathbf{V}\mathbf{V}^{\mathrm{T}}\mathbf{X}_S \quad (27)$$

with $\bar{\mathbf{K}} = \mathbf{K} + k_m\mathbf{V}\mathbf{V}^{\mathrm{T}}$, averaged total stiffness matrix.

Assuming that there is a unique static deflection, i.e., $\bar{\mathbf{K}}$ is invertible (this condition was not satisfied by the semi-definite system (15)), a development based on a fixed-point method can be

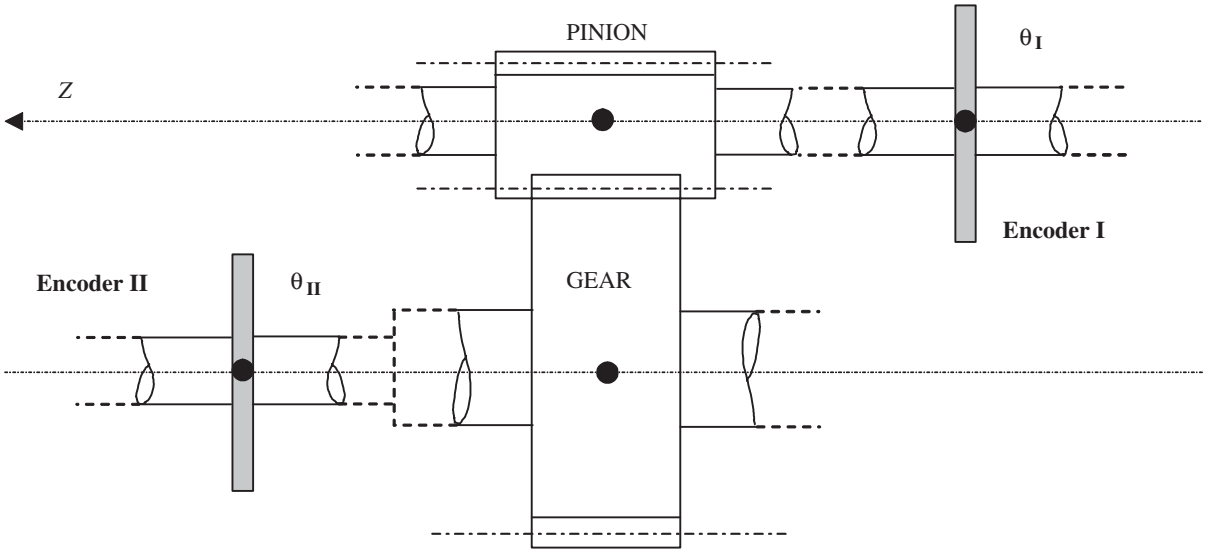

Fig. 3. Positions of the section of reference (or encoders) for the definition of transmission errors.

used since $\alpha \prec 1$. The corresponding recursive expression, at iteration r, reads

$$\mathbf{X}_S^{(r)} = \mathbf{X}_0 + \left[\left(\sum_i k_i \delta e(M_i)\right) - \alpha k_m g(\vartheta)\mathbf{V}^{\mathrm{T}}\mathbf{X}_S^{(r-1)}\right]\mathbf{C}_V \tag{28}$$

with $\mathbf{X}_0 = \bar{\mathbf{K}}^{-1}\mathbf{F}_0$, the static solution with averaged mesh stiffness; $\mathbf{C}_V = \bar{\mathbf{K}}^{-1}\mathbf{V}$, which indicates that $\mathbf{X}_S$ is of the form

$$\mathbf{X}_S = \mathbf{X}_0 + \varphi(\vartheta)\mathbf{C}_V \tag{29}$$

where $\varphi(\vartheta)$ is an unknown scalar function depending on time, on tooth shape deviations and errors through $\left(\sum_i k_i \delta e(M_i)\right)$, etc.

From the expression of the quasi-static transmission error under load (10), one obtains:

$$\mathrm{TE}_S = w_{x0} + \varphi(\vartheta)C_{wv} + \mathrm{NLTE}, \tag{30}$$

with $w_{x0} = \mathbf{W}^T\mathbf{X}_0$, $C_{wv} = \mathbf{W}^T\bar{\mathbf{K}}^{-1}\mathbf{V}$, from which, $\varphi(\vartheta)$ is deduced as

$$\varphi(\vartheta) = \frac{\mathrm{TE}_S - w_{x0} - \mathrm{NLTE}}{C_{wv}} \tag{31}$$

and the quasi-static solution can be expressed in terms of transmission errors as

$$\mathbf{X}_S = \mathbf{X}_0 + \frac{\mathrm{TE}_S - w_{x0} - \mathrm{NLTE}}{C_{wv}}\mathbf{C}_v. \tag{32}$$

4.3. Some analytical results

In the appendix, some original analytical results and properties about the terms C_{vv}, C_{wv}, v_{x0}, etc. in the above equations are established. The most important formulae are listed as follows:

$$C_{vv} = \frac{1}{k_m}, \tag{33}$$

$$v_{x0} = \widehat{v}_{x0} = \frac{F_s}{k_m}, \tag{34}$$

$$C_{wv} = \frac{v_{x0}}{F_s \cos\beta_b} = \frac{1}{k_m \cos\beta_b}, \tag{35}$$

$$v_{xs} = v_{x0} + \cos\beta_b(\mathrm{TE}_S - \mathrm{NLTE} - w_{x0}). \tag{36}$$

4.4. Equation for dynamic tooth load

Neglecting viscous forces, the general expression of the dynamic mesh force is

$$F_D = \sum_i k_i\left[\mathbf{V}^T\mathbf{X} - \delta e(M_i)\right] = k_m(1 + \alpha g(\vartheta))\mathbf{V}^T\mathbf{X} - \sum_i k_i \delta e(M_i). \tag{37}$$

Replacing expression (32) of $\mathbf{X}_S$ in the quasi-static equations (27) leads to the following

$$\bar{\mathbf{K}}\left[\mathbf{X}_0+\frac{\mathrm{TE}-\mathrm{NLTE}-w_{x0}}{C_{wv}}\mathbf{C}_v\right]+\alpha k_m g(\vartheta)\left[v_{x0}+\frac{\mathrm{TE}-\mathrm{NLTE}-w_{x0}}{C_{wv}}\mathbf{C}_{vv}\right]\mathbf{V}$$
$$=\mathbf{F}_0+\left(\sum_i k_i\delta e(M_i)\right)\mathbf{V}, \tag{38}$$

where $v_{x0}=\mathbf{V}^T\mathbf{X}_0$, $C_{vv}=\mathbf{V}^T\bar{\mathbf{K}}^{-1}\mathbf{V}$, which after simplification, results in

$$\sum_i k_i\delta e(M_i)=\frac{\mathrm{TE}_S-w_{x0}-\mathrm{NLTE}}{C_{wv}}(1+\alpha k_m g(\vartheta)C_{vv})+\alpha k_m v_{x0}g(\vartheta) \tag{39}$$

and leads to the dynamic force equation when re-injected in Eq. (37):

$$F_D=k_m v_x-\frac{\mathrm{TE}_S-w_{x0}-\mathrm{NLTE}}{C_{wv}}(1+\alpha k_m g(\vartheta)C_{vv})+\alpha k_m g(\vartheta)(v_x-v_{x0}), \tag{40}$$

where $v_x=\mathbf{V}^{\mathrm{T}}\mathbf{X}$.

Using Eqs. (33)–(36), the total dynamic mesh force F_D can be finally re-written in a simple form very close to the sdof Eq. (24) as

$$F_D=F_S+k_m(1+\alpha g(\vartheta))v_{xD}, \tag{41}$$

where $v_{xD}=\mathbf{V}^{\mathrm{T}}\mathbf{X}_D$ and $\mathbf{X}_D=\mathbf{X}-\mathbf{X}_S$ represents the dynamic displacement vector.

4.5. Equations of motion in terms of transmission errors

Combining the results in Sections 4.2, 4.3 and 4.4 and introducing a viscous damping matrix $[C]$, Eq. (26) can be transformed after some manipulations into

$$\Omega_1^2\mathbf{M}\mathbf{X}''+\Omega_1\mathbf{C}\mathbf{X}'+\left[\bar{\mathbf{K}}+\alpha k_m g(\vartheta)\mathbf{V}\mathbf{V}^{\mathrm{T}}\right]\mathbf{X}$$
$$=\mathbf{F}_0+\left[k(\vartheta)\cos\beta_b(\mathrm{TE}_s-\mathrm{NLTE}-w_{x0})+\alpha F_S g(\vartheta)\right]\mathbf{V}$$
$$-\Omega_1^2[\mathrm{NLTE}''\,\mathbf{E}(\vartheta)+\mathrm{NLTE}'\,\mathbf{F}(\vartheta)+\mathbf{G}(\vartheta)]. \tag{42}$$

As for the sdof system, the quasi-static and dynamic displacements can be separated as

$$\mathbf{X}=\mathbf{X}_S+\mathbf{X}_D. \tag{43}$$

Using Eq. (35) and noting from Eqs. (A.2a) and (A.2b) (see the Appendix) that $\widehat{\mathbf{X}}_0=F_S\mathbf{C}_v$, the nth derivatives with respect to the angular variable ϑ of the quasi-static vector in (32) are

$$\mathbf{X}_S^{(n)}=\frac{\cos\beta_b}{v_{x0}}(\mathrm{TE}_S-\mathrm{NLTE})^{(n)}\widehat{\mathbf{X}}_0 \tag{44}$$

and the dynamic displacements appear as the solutions of the differential system:

$$\begin{aligned}&\Omega_1^2\mathbf{M}\mathbf{X}_D'' + \Omega_1\mathbf{C}\mathbf{X}_D' + \left[\bar{\mathbf{K}} + \alpha k_m g(\vartheta)\mathbf{V}\mathbf{V}^T\right]\mathbf{X}_D \\ &\quad = \frac{-\cos\beta_b\Omega_1^2}{v_{x0}}\mathrm{TE}_S''\mathbf{M}\widehat{\mathbf{X}}_0 - \frac{\cos\beta_b\Omega_1}{v_{x0}}\mathrm{TE}_S'\mathbf{C}\widehat{\mathbf{X}}_0 \\ &\qquad + \frac{\cos\beta_b\Omega_1}{v_{x0}}\mathrm{NLTE}'\mathbf{C}\widehat{\mathbf{X}}_0 - \Omega_1^2\left[\mathrm{NLTE}''\left[\mathbf{E}(\vartheta) - \frac{\cos\beta_b}{v_{x0}}\mathbf{M}\widehat{\mathbf{X}}_0\right] + \mathrm{NLTE}'\mathbf{F}(\vartheta) + \mathbf{G}(\vartheta)\right].\end{aligned} \tag{45}$$

5. Approximate equations

In order to qualitatively appraise the contributions of the various excitation terms, an approximate approach to the solution is proposed. There is no exact solution to the parametrically excited differential Eqs. (20) and (21) or the differential systems (42) and (45) but approximate equations of motion can be obtained by using a perturbation method [11,12]. Assuming that $\alpha \prec\prec 1$ (this assumption being more suited to helical gears), particular stable solutions can be sought as asymptotic expansions of the form

$$x = \mathrm{TE} - \mathrm{NLTE} = x_{(0)} + \alpha x_{(1)} + \alpha^2 x_{(2)} + \cdots, \tag{46a}$$

$$x_D = x_{D(0)} + \alpha x_{D(1)} + \alpha^2 x_{D(2)} + \cdots \tag{46b}$$

or

$$\mathbf{X} = \mathbf{X}_{(0)} + \alpha\mathbf{X}_{(1)} + \alpha^2\mathbf{X}_{(2)} + \cdots, \tag{46c}$$

$$\mathbf{X}_D = \mathbf{X}_{D(0)} + \alpha\mathbf{X}_{D(1)} + \alpha^2\mathbf{X}_{D(2)} + \cdots. \tag{46d}$$

The identification of the main order expressions leads to the following sets of equations depending on the nature of the unknowns (total or dynamic displacements) and on the model:

(a) *sdof torsional models*

$$\Omega_1^2 m_{\mathrm{eq}}x_{(0)}'' + \Omega_1 c x_{(0)}' + k_m\cos^2\beta_b x_{(0)} = k_m\cos^2\beta_b[\mathrm{TE}_S - \mathrm{NLTE}] - \Omega_1^2\frac{J_2}{\mathrm{Rb}_2^2}\mathrm{NLTE}'', \tag{47a}$$

$$\Omega_1^2 m_{\mathrm{eq}}x_{D(0)}'' + \Omega_1 c x_{D(0)}' + k_m\cos^2\beta_b x_{D(0)} = -m_{\mathrm{eq}}\Omega_1^2\left[\mathrm{TE}_S'' + \frac{J_2}{J_1}\frac{\mathrm{Rb}_1^2}{\mathrm{Rb}_2^2}\mathrm{NLTE}''\right]. \tag{47b}$$

(b) *3D models*

$$\begin{aligned}&\Omega_1^2\mathbf{M}\mathbf{X}_{(0)}'' + \Omega_1\mathbf{C}\mathbf{X}_{(0)}' + \bar{\mathbf{K}}\mathbf{X}_{(0)} \\ &\quad = \mathbf{F}_0 - k_m\cos\beta_b w_{x0}\mathbf{V} + k_m\cos\beta_b(\mathrm{TE}_S - \mathrm{NLTE})\mathbf{V} \\ &\qquad - \Omega_1^2[\mathrm{NLTE}''\mathbf{E}(\vartheta) + \mathrm{NLTE}'\mathbf{F}(\vartheta) + \mathbf{G}(\vartheta)].\end{aligned} \tag{48a}$$

$$\Omega_1^2\mathbf{M}\mathbf{X}''_{D(0)}+\Omega_1\mathbf{C}\mathbf{X}'_{D(0)}+[\,]\bar{\mathbf{K}}\mathbf{X}_{D(0)}$$
$$=\frac{-\cos\beta_b\Omega_1^2}{v_{x0}}\mathrm{TE}''_S\mathbf{M}\widehat{\mathbf{X}}_0-\Omega_1^2\left[\mathrm{NLTE}''\left[\mathbf{E}(\vartheta)-\frac{\cos\beta_b}{v_{x0}}\mathbf{M}\widehat{\mathbf{X}}_0\right]+\mathrm{NLTE}'\,\mathbf{F}(\vartheta)+\mathbf{G}(\vartheta)\right]. \quad (48b)$$

6. Numerical results—Assessment of transmission error-based formulations

In this section, the validity and limits of the proposed excitation models are examined by comparing the numerical solutions of the general form in Eq. (14) and of the differential systems with transmission errors as forcing terms. Because of the errors induced by numerical differentiation, the formulation based on dynamic displacements and second-order time derivatives of the quasi-static transmission error under load TE_S is not suited for numerical integration and will be considered for qualitative discussions only.

6.1. Model

The geared drive under consideration is the one used in a series of experiments and simulations by Baud and Velex [16]. It consists of a single-stage spur or helical geared drive with noticeable contributions of bending–torsion couplings which make it impossible to model as a purely torsional system. Gear geometries (including profile modifications) as well as bearing stiffnesses are defined in Tables 1 and 2 and in Fig. 4, the pitch error distribution (on the pinion only) is shown in Fig. 5. The dynamic model of the test gear–shaft–bearing system is shown in Fig. 6; it comprises 40 elements (including a pinion–gear element) with 258 dof. The tooth mesh model is based on the analytical formulae of Weber and Banaschek [17] and O'Donnell [18]. A constant torque of 254.8 N m is applied at the motor (on the pinion shaft) and the resisting load is given by a torsional stiffness at one free end of the gear shaft. Two different damping levels are introduced through a unique modal damping factor of 0.03 and 0.1, respectively.

Table 1
Gear data

	Pinion	Gear
Module (mm)	4	
Tooth number	26	157
Pressure angle (deg)	20	
Helix angle (deg)	0 or 20	
Addendum coefficient	1	1
Dedendum coefficient	1.46	1.46
Profile shift coefficient	0.16	−0.16
Face width (mm)	50	40
Tip relief amplitude P_c (μm)	13.3	13.3
Extent of profile modification L_c (% of the nominal active profile)	0.2 (short) 0.5 (long)	0.2 (short) 0.5 (long)

Table 2
Bearing data

Node	Stiffness in the S direction (N/m)	Stiffness in the S direction (N/m)	Stiffness in the Z direction (axial) (N/m)
5	1E9	1E9	0
9	1E9	1E9	0
13	0	0	3.5 E7
23	7E7	7E7	0
25	7E7	7E7	0
33	1E9	1E9	0
37	1E9	1E9	0
41	0	0	6E7

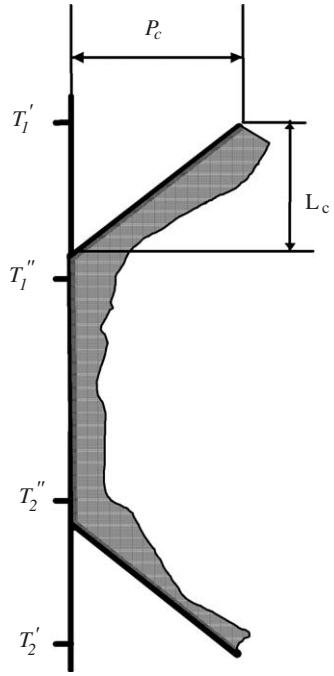

Fig. 4. Definition of profile modifications (P_c is the tip relief amplitude, and L_c is the extent of modification measured on the base plane).

6.2. Numerical solutions

Time-step integrations based on the Newmark method combined with a normal contact algorithm [10] are used for solving the following:

(i) The general form of the equations of motion (14), whose results compare well with the experimental evidence from a highly instrumented single-stage spur and helical gear test rig as shown in Ref. [16] and which will be subsequently used as references. Eq. (14) accounts for mesh

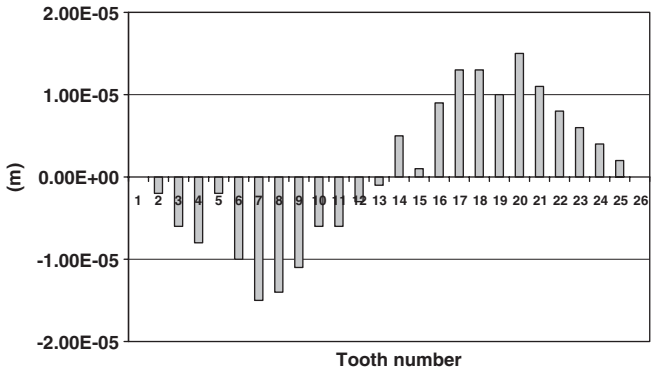

Fig. 5. Cumulative pitch error distribution on the pinion.

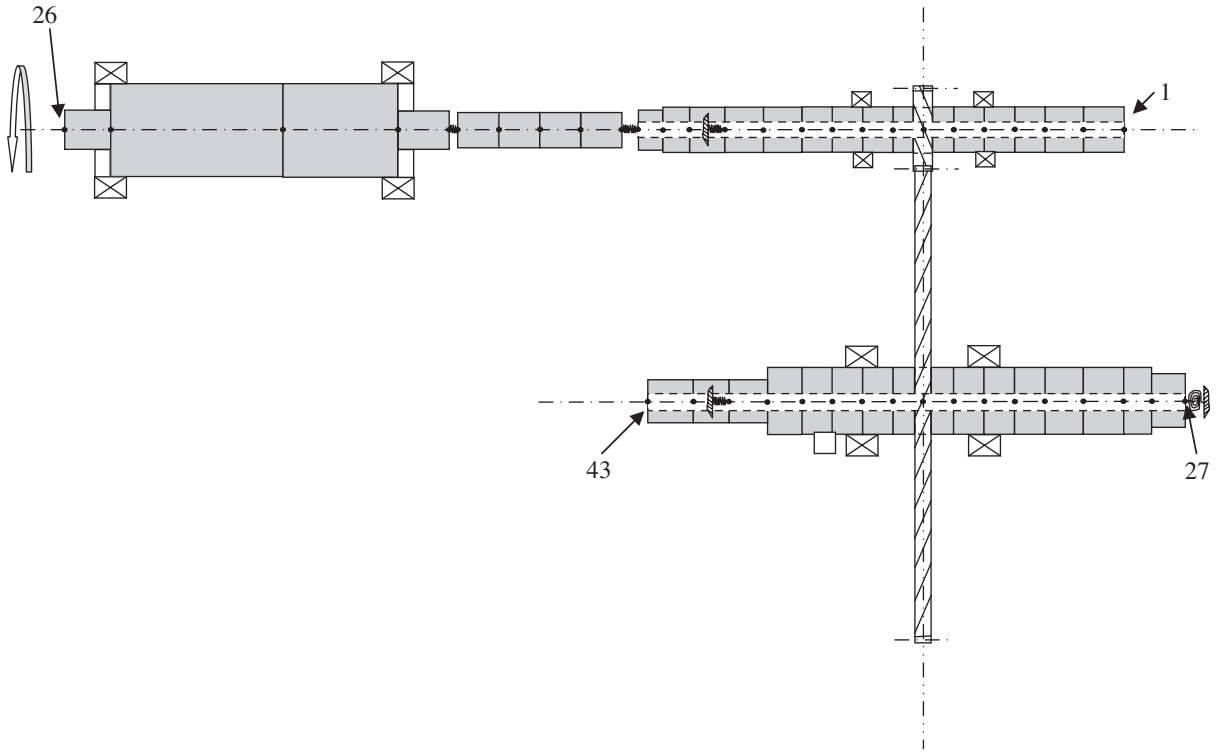

Fig. 6. Finite element model of the geared unit.

stiffness parametric excitations, the contributions of tooth shape deviations and/or errors as well as the possible effects of backlash and tooth separation.

(ii) The differential system (42) in which excitations are introduced via quasi-static transmission error under load, no-load transmission error and its time-derivatives and time-varying mesh stiffness.

(iii) The main order approximate system (48a) where a constant stiffness matrix is employed and which can be considered as a generalized form of the formulation proposed by Özgüven and Houser [19].

Note that the contact algorithm is applied in all cases so that the time-varying stiffness matrix in Eqs. (14) and (42) as well as the average stiffness matrix in Eq. (48a) are evaluated at each step depending on the instantaneous contact conditions between the mating teeth. Finally, the quasi-static transmission error TE_S and the no-load transmission error NLTE needed as parts of the forcing terms in Eqs. (42) and (48a) are determined by solving Eq. (14) for a very low speed and for the positions of the encoders (or nodes of reference) corresponding to position 1, as defined in

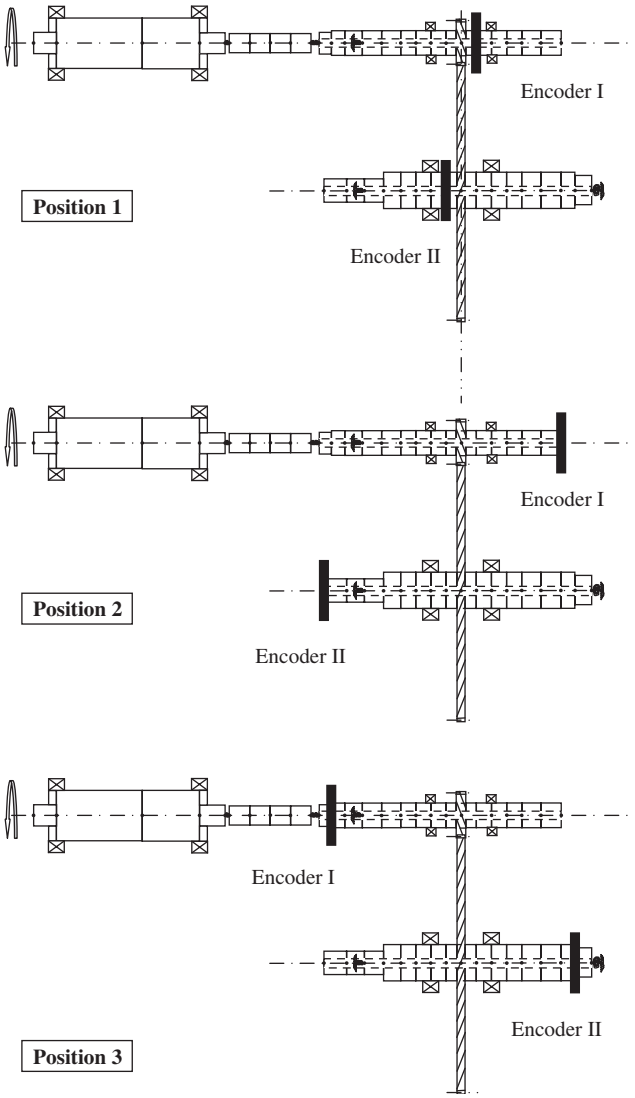

Fig. 7. Positions of encoders for transmission error calculations.

Fig. 7. It is clear that this numerical approach to excitations in no way precludes the use of experimental transmission error measurements for generating the forcing terms in Eqs. (42) and (48a).

6.3. Results

6.3.1. Spur gears—short tip relief (Table 1), NLTE = 0

The first set of response curves in Figs. 8a–c [NB: 'Reference' in Figs. 8–13 stands for solutions obtained by numerical integration of Eq. (14)] was obtained for a modal damping factor of 0.03. A high degree of agreement was found between the three solution methodologies except near the major tooth critical speed where contacts between the teeth were momentarily lost and shocks occurred. In such conditions, the hypothesis of similar contact conditions in both dynamic and quasi-static regimes (see Eqs. (18) and (25)–(26)) was not verified and the transmission error-based formulations were unable to correctly account for the amplitude jumps associated with these contact losses. The latter emphasizes the need for including nonlinearities in gear dynamic models particularly in the case of lightly damped spur gears. For a larger damping level (modal damping factor of 0.1), the results were better and even the solutions derived from the perturbation method at the main order look reasonably satisfactory (Figs. 9a–c).

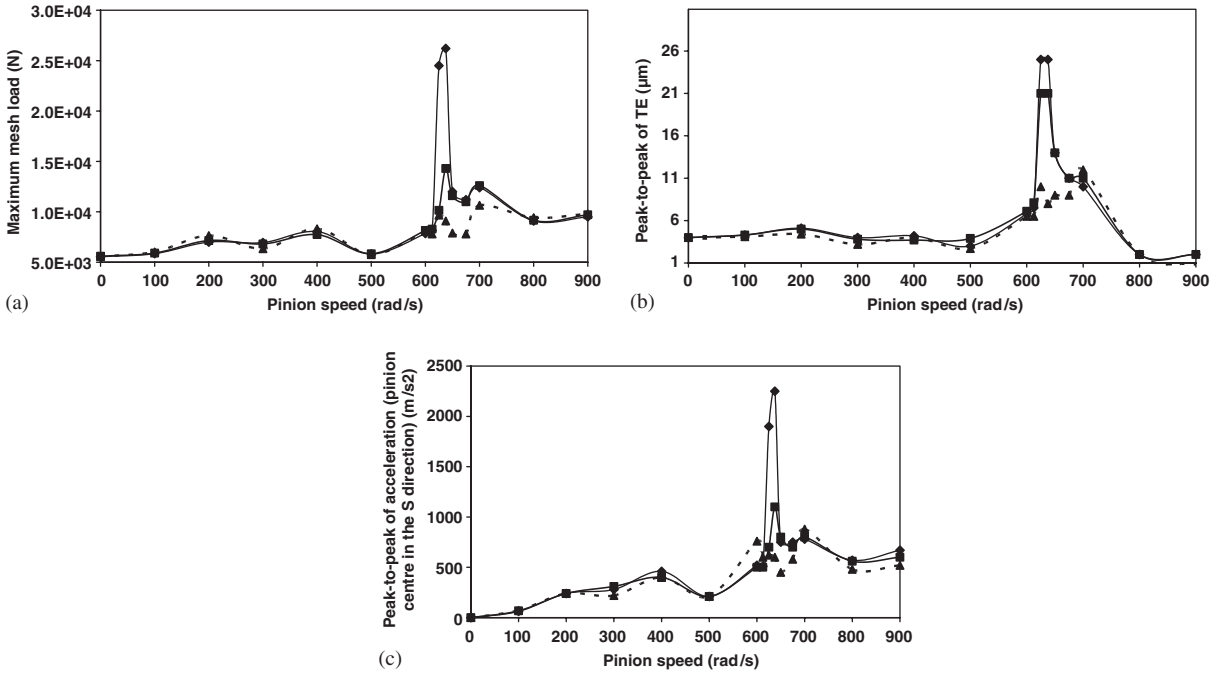

Fig. 8. Comparisons between the response curves from the solution of reference and the formulations based on transmission errors (spur gear, modal damping factor of 0.03, short profile modifications, no pitch error) (a) maximum dynamic tooth load versus pinion speed, (b) peak-to-peak of dynamic transmission error versus pinion speed, (c) peak-to-peak of the acceleration at the pinion centre in the S direction versus pinion speed. —◆—, reference; —■—, from Eq. (42) (TE-based equations); – ▲ –, from Eq. (48a) (main order perturbation).

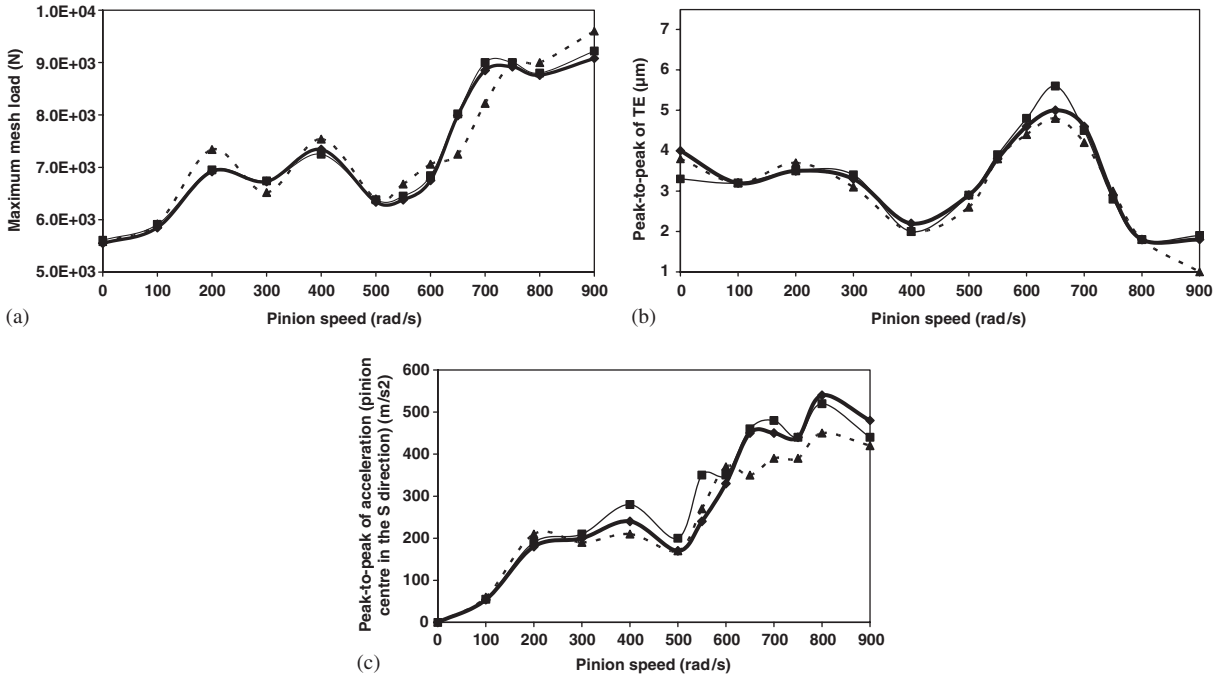

Fig. 9. Comparisons between the response curves from the solution of reference and the formulations based on transmission errors (spur gear, modal damping factor of 0.1, short profile modifications, no pitch error) (a) maximum dynamic tooth load versus pinion speed, (b) peak-to-peak of dynamic transmission error versus pinion speed, (c) peak-to-peak of the acceleration at the pinion centre in the S direction versus pinion speed. —◆—, reference; —■—, from Eq. (42) (TE-based equations); – ▲ –, from Eq. (48a) (main order perturbation).

6.3.2. *Spur gears—long tip relief (Table 1),* NLTE$\neq$0

Here again, a very close agreement was observed (Figs. 10a–c) when comparing the response curves delivered by the numerical integration of Eq. (42) and that of the equations of reference (14). Moreover, the importance of NLTE″ in this particular case with long profile reliefs was highlighted, particularly in the vicinity of tooth critical speeds. It was observed that when NLTE″ was set at zero in the equations of motion, the dynamic responses were significantly different from the reference curves. This phenomenon is indeed illustrated by the three examples of instantaneous mesh force signals at 100, 400 and 800 rad/s on the pinion shaft in Fig. 11.

6.3.3. *Spur gears—short tip relief and pitch errors on the pinion (Table 1 and Fig. 5),* NLTE$\neq$0

A more realistic situation was considered with the introduction of pitch errors in the simulations. The tooth load, dynamic transmission error and acceleration curves in Figs. 12a, b and c, respectively, show the soundness of the proposed formulations. However, the results derived from the main order approximation of the perturbation method (48a) appear as less accurate near critical speeds. It was also observed that the influence of NLTE″ is less pronounced than in the case of long reliefs in Section 6.3.2 (Fig. 10).

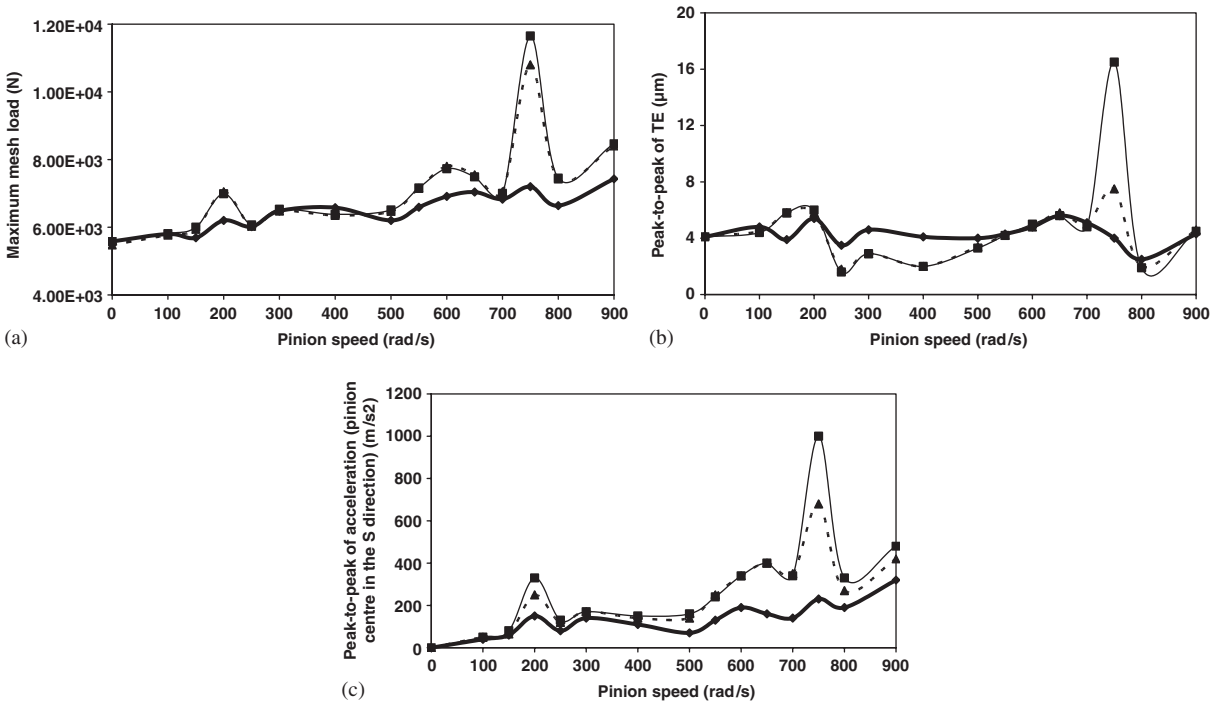

Fig. 10. Influence of no-load transmission error—comparisons between the response curves from the solution of reference and the formulations based on transmission errors (spur gear, modal damping factor of 0.1, long profile modifications, no pitch error): (a) maximum dynamic tooth load versus pinion speed, (b) peak-to-peak of dynamic transmission error versus pinion speed, (c) peak-to-peak of the acceleration at the pinion centre in the S direction versus pinion speed. —◆—, TE-based formulation (with NLTE = 0; —■—, from Eq. (42) (TE-based formulation); – ▲ –, reference.

6.3.4. *Helical gears—short tip relief and pitch errors on the pinion (Table 1 and Fig. 5),* NLTE$\neq$0

The tooth profiles were modified as indicated in Table 1 and the same cumulative pitch error distribution as for the spur gear example was introduced. Simulations were conducted for the lowest damping factor of 0.03. Figs. 13a–c show that, generally speaking, the dynamic response curves by the method of reference and the method based on transmission errors accord well, while the solutions by the truncated perturbation method are less satisfactory (although helical gears generate lower mesh stiffness variations).

6.3.5. *Positions of the nodes or section of reference for the definition of* TE_S

The final test dealt with the validity of the correction factor w_{x0} in Eqs. (42) and (48a) which is the only parameter accounting for the positions of the virtual or real encoders in the definition of transmission errors. Three different combinations of positions were considered; they are schematically represented in Fig. 7. The corresponding force and acceleration time signals were calculated over the whole speed range (from quasi-static conditions to 900 rad/s on the pinion shaft). All results were superimposed and proved that the modification by w_{x0} is sound and that the calculated dynamic forces and accelerations are independent of

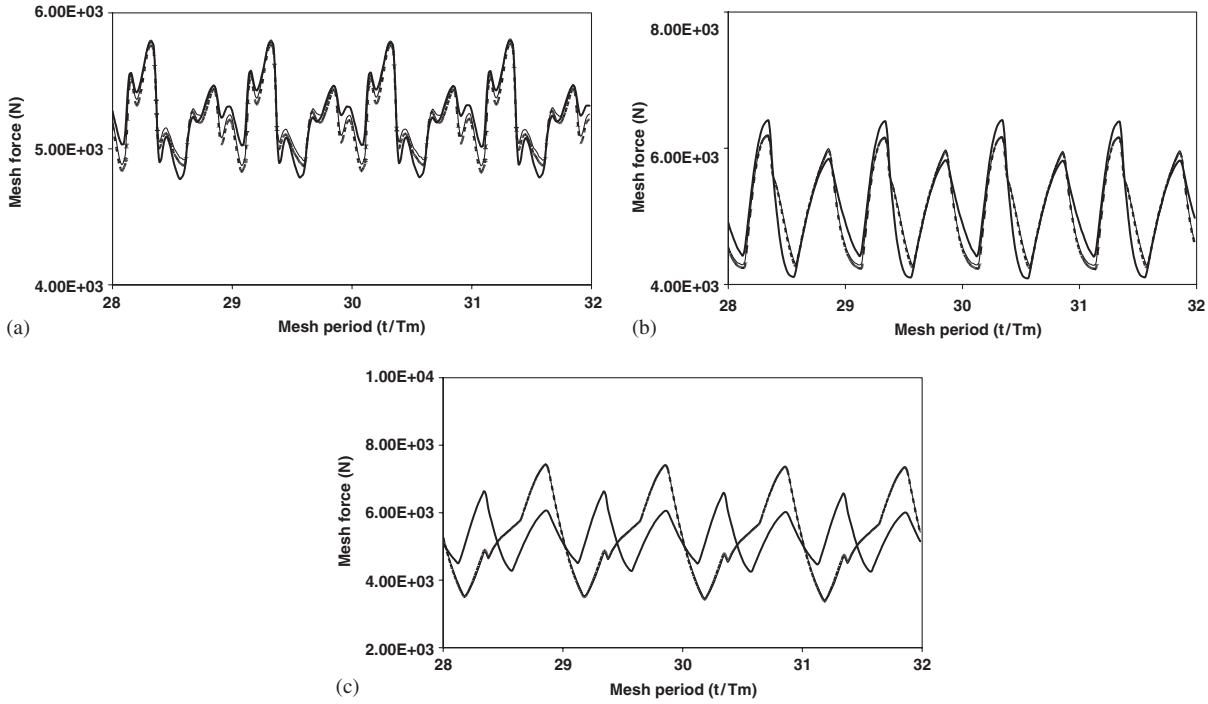

Fig. 11. Influence of no-load transmission error—instantaneous total mesh force at three different speeds (spur gear, modal damping factor of 0.1, long profile modifications, no pitch error, t/Tm is the normalized time with respect to the mesh period, Tm): (a) pinion speed of 100 rad/s, (b) pinion speed of 400 rad/s, (c) pinion speed of 800 rad/s. ▬▬, TE-based formulation (with NLTE = 0); ——, from Eq. (42) (TE-based formulation); – – –, reference.

the section of reference (or encoder positions) used in transmission error calculations (or measurements).

7. Discussion—closure

Some original equations were presented which make it possible to simulate gear excitations from simulated or measured transmission errors. The validity of the proposed formulations was confirmed by numerous comparisons with the results delivered by the equations of reference (14) for both spur and helical gears.

Based on the analytical developments, the inter-dependence was clarified between the excitations associated with a pinion–gear pair in mesh and the corresponding quasi-static transmission error under load and no-load transmission error. It was demonstrated that, if there is a similarity in the structure of the equations of motion for the sdof torsional model (20) and (21), and the 3D axial–torsional–flexural models (42) and (45), several additional terms in the latter equations prevent direct transposition of the torsional formulation onto 3D models. However, it can be proved that the additional excitation components vanish when the system controlled by

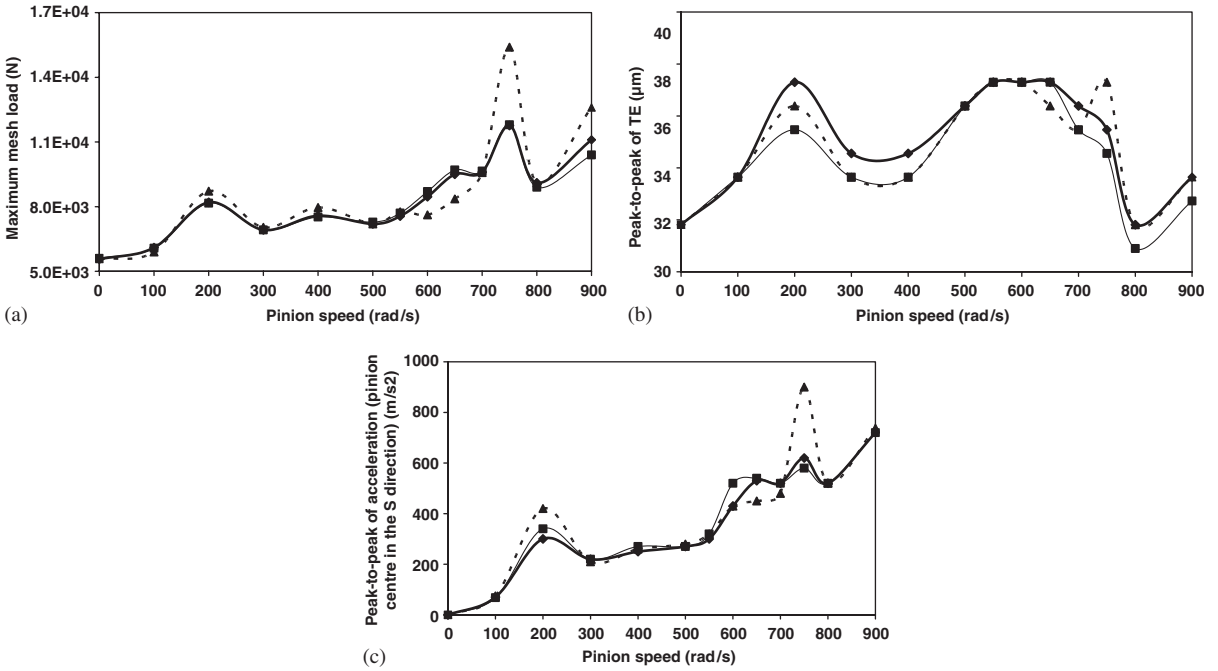

Fig. 12. Comparisons between the response curves from the solution of reference and the formulations based on transmission errors (spur gear, modal damping factor of 0.1, short profile modifications, pitch errors on pinion): (a) maximum dynamic tooth load versus pinion speed, (b) peak-to-peak of dynamic transmission error versus pinion speed, (c) peak-to-peak of the acceleration at the pinion centre in the S direction versus pinion speed. —◆—, reference; —■—, from Eq. (42) (TE-based equations); – ▲ –, from Eq. (48a) (main order perturbation).

Eq. (42) is reduced to the torsional model of Section 3. From Eq. (20), these additional terms read

$$\mathbf{F}_0 + \left[-\mathbf{W}^{\mathrm{T}}\mathbf{X}_0 k(\vartheta)\cos\,\beta_b + \alpha F_S g(\vartheta)\right]\mathbf{V}, \tag{49}$$

In the particular case of the simple torsional model, one has

$$\mathbf{V} = \cos\,\beta_b \mathbf{W} \tag{50}$$

such that after simplifying with Eq. (34) Eq. (49) becomes:

$$\mathbf{F}_0 - F_S\mathbf{V} = \begin{bmatrix} C_{m0} \\ C_r \end{bmatrix} - F_t \begin{bmatrix} \mathrm{Rb}_1 \\ \mathrm{Rb}_2 \end{bmatrix} = \begin{bmatrix} 0 \\ 0 \end{bmatrix}. \tag{51}$$

Another significant difference between the two models comes from the excitation vectors $\mathbf{F}(\vartheta), \mathbf{G}(\vartheta)$, which are not directly related to transmission errors, and for example, account for imbalances induced by pinion and gear eccentricities which can generate severe bending vibrations.

It has also been proved that the quasi-static transmission error under load TE_S actually contributes to the dynamic system excitations; nevertheless, the major time-varying forcing terms, when considering elastic displacements as the unknowns in Eqs. (42), (48a) and (48b), depend mostly on the difference between TE_S and the no-load transmission error NLTE, and not on TE_S

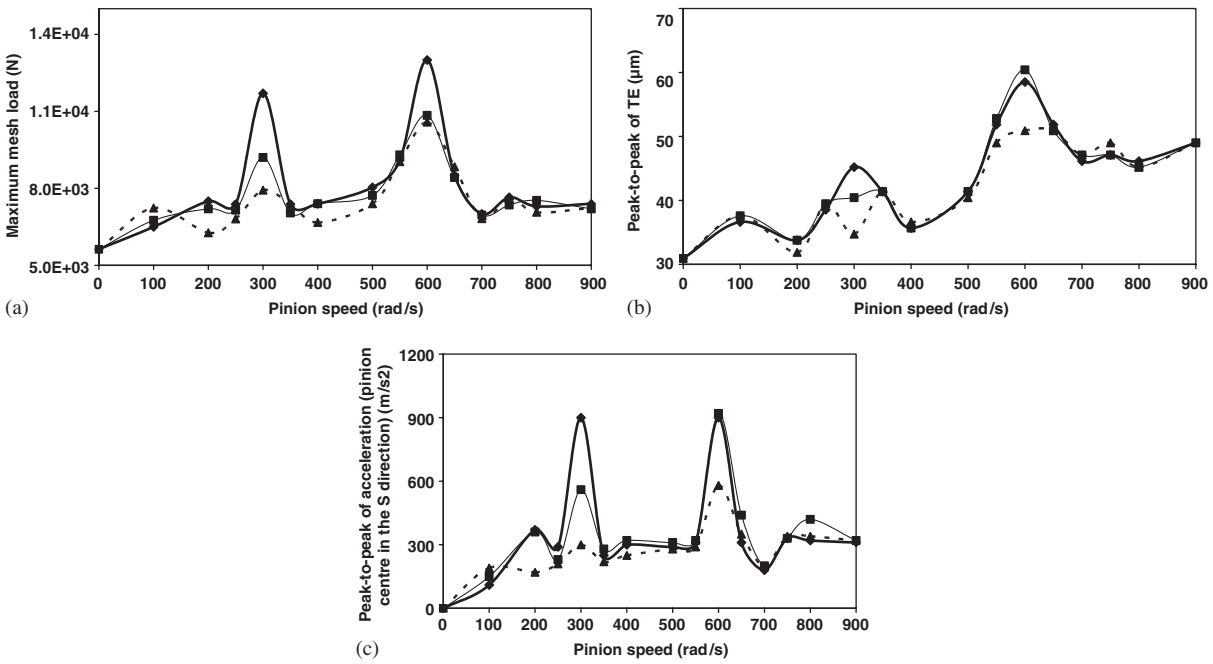

Fig. 13. Comparisons between the response curves from the solution of reference and the formulations based on transmission errors (Helical gear, modal damping factor of 0.03, short profile modifications, pitch errors on pinion): (a) maximum dynamic tooth load versus pinion speed, (b) peak-to-peak of dynamic transmission error versus pinion speed, (c) peak-to-peak of the acceleration at the pinion centre in the S direction versus pinion speed. —◆—, reference; —■—, from Eq. (42) (TE-based equations); – ▲ –, from Eq. (48a) (main order perturbation).

only. Note that, in contrast to the sdof model, NLTE cannot be transferred from the right-hand side of the differential system to the dof vector. One of the reasons is that the forcing term $k(\vartheta)\cos\beta_b(\mathrm{TE}_s - \mathrm{NLTE})$ in Eq. (42) (and similarly $k_m\cos\beta_b(\mathrm{TE}_s - \mathrm{NLTE})$ in Eq. (48a)) applies only to the non-zero components of the structure vector $\mathbf{V}$, i.e., the pinion–gear displacements and rotations, and not to all dof. Consequently, it is found that, for 3D models, NLTE excitations cannot be implicitly included in the dof.

The time derivatives of no-load transmission errors appear as additional excitations whose contributions increase with speed and also depend on the nature of tooth deviations/errors. The spectral contents of NLTE comprise mostly:

(a) low-frequency components associated with eccentricities, envelopes of cumulative pitch errors, etc., whose contributions in terms of time derivatives of NLTE are moderate,

(b) higher frequencies associated with individual tooth deviations i.e., the mesh frequency and its harmonics, having amplitudes generally lower than those associated with low frequencies (with the noticeable exception of long profile reliefs on conventional spur gears).

Therefore, for most practical conditions, the excitation levels generated by the time derivatives of no-load transmission error are less important than those due to the quasi-static transmission error under load TE_S or (TE_S−NLTE).

The equations derived from a perturbation method are proved to be reasonable approximations leading to acceptable solutions in most cases. It can be noticed that time-varying mesh stiffness or

time-varying mesh stiffness matrices do not explicitly appear in Eqs. (47) and (48) but are implicitly taken into account via transmission errors. Neglecting the forcing terms proportional to NLTE′ or NLTE″ in the equations in terms of dynamic displacements Eqs. (47b) and (48b), it becomes clear that the time variations of TE_S are key factors which largely contribute to the dynamic behaviour since the only possible excitation at the main order is TE''_S. From the latter, it can be deduced that minimizing the fluctuations of quasi-static transmission error under load reduces displacements and, via Eqs. (24) and (41), reduces dynamic tooth loads.

From a fundamental viewpoint, all the theoretical developments on 3D models rely on the assumption that the averaged total stiffness matrix $\bar{\mathbf{K}}$ can be inverted. With regard to this condition of a unique 'averaged' static deformed shape, the torsional displacements can be troublesome because they can be defined at a constant. However, since these angles represent elastic components superimposed on rigid-body large rotations, it is possible to choose any arbitrary angular datum on the pinion or the gear shaft and resolve the above-mentioned difficulty. Another fundamental hypothesis consists in the substitution of the position-dependent structure vector $\mathbf{V}(\mathbf{M}_i)$ by a constant structure vector. For narrow-faced gears, this constraint is certainly acceptable without significant influence on dynamic responses (see for instance the discussion about the iterative spectral method in Ref. [20] which partly relies on this approximation). In the case of wide-faced gears, all the components of the structure vector actually depend on the potential point of contact under consideration because of gear body deflections (mainly torsion and bending) [21]. In these conditions, none of the theoretical developments in Section 4 is possible anymore and no analytical formulation has been found for gear excitations in terms of transmission errors only. Further work is certainly needed in this area, but it seems that the concept of transmission errors as excitations or as excitation-related parameters is more suited to narrow-faced gears.

Appendix A. Some analytical results

A.1. Expression of $C_{vv} = \{V\}^{\mathrm{T}}\left[\bar{K}\right]^{-1}\{V\}$

The averaged structure vector $\{V\}$ can be expressed as

$$\{V\}^{\mathrm{T}} = (\mathbf{n}, \mathbf{O}_1\mathbf{M}_0 \times \mathbf{n}, -\mathbf{n}, -\mathbf{O}_2\mathbf{M}_0 \times \mathbf{n}) \tag{A.1}$$

and is proportional to the coordinates of the mesh force wrenches (see for instance Ref. [22] for a review on the theory of screws and wrenches) on the pinion in O_1 and on the gear in O_2 when the mesh force distribution is reduced to a single sliding vector applied along a line (M_0,**n**) fixed in space. (A discussion about the reduction of the mesh force wrench to a sliding vector and about the position of its line of action can be found in Ref. [15]). Therefore, the quantity $F_S\{\mathrm{V}\}$ represents the set of external forces and moments in O_1 and O_2 generated by a mesh force F_S as shown in Fig. A1 (note that the system is in equilibrium).

Consequently, C_{vv} can be re-written in the form:

$$C_{vv} = \frac{1}{F_S}\{V\}^{\mathrm{T}}\left[\left[\bar{K}\right]^{-1}F_S\{V\}\right] = \frac{1}{F_S}\{V\}^{\mathrm{T}}\left\{\widehat{X}_0\right\}, \tag{A.2}$$

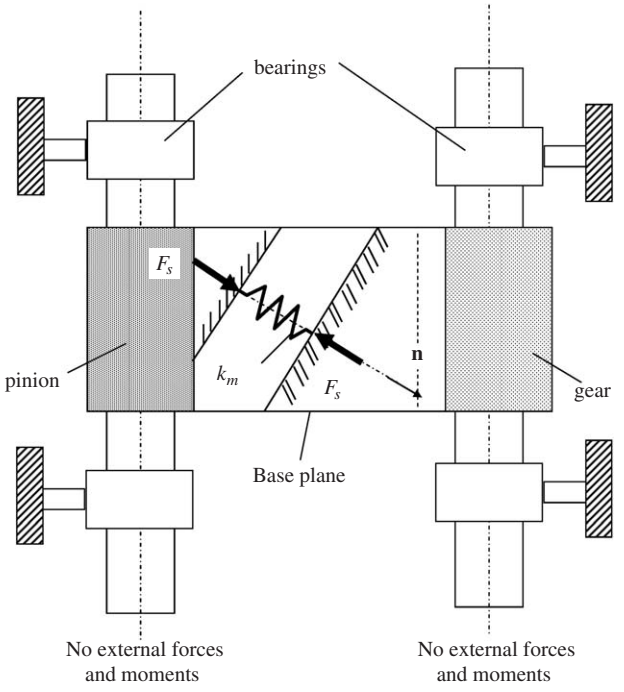

Fig. A1. Loading conditions associated with the static deflection vector $\left\{\widehat{X}_0\right\}$.

where $\left\{\widehat{X}_0\right\} = \left[\bar{K}\right]^{-1} F_S\{V\}$ is the static deflection vector associated with the loading conditions shown in Fig. A1.

$\{V\}^{\mathrm{T}}\left\{\widehat{X}_0\right\}$ therefore represents the mesh (spring) deflection δ_{ms} in the normal direction **n**, thus one obtains:

$$C_{vv} = \frac{\delta_{ms}}{F_S} = \frac{1}{k_m}. \tag{A.3}$$

A.2. Relations between $\left\{\widehat{X}_0\right\}$ *and* $\{X_0\}$*:*

Both vectors represent static deflections of the geared system with the difference that $\left\{\widehat{X}_0\right\}$ is obtained with the mesh force as the only force applied to the geared unit (the realism of the situation in Fig. A1 is not discussed here), while $\{X_0\}$ is the static deflection vector when constant torsional torques are applied on the pinion shaft and on the gear shaft (which induce the same force F_S at the mesh interface). From this observation, the following properties can be established:

(a) $\{V\}^{\mathrm{T}}\left\{\widehat{X}_0\right\}$ and $\{V\}^{\mathrm{T}}\{X_0\}$ represent the static mesh deflection under the same load F_S consequently

$$\{V\}^{\mathrm{T}}\{X_0\} = \{V\}^{\mathrm{T}}\left\{\widehat{X}_0\right\} \tag{A.4}$$

or using the abridged notations

$$v_{x0} = \widehat{v}_{x0} = \frac{F_S}{k_m}. \tag{A.5}$$

(b) Referring to Fig. A1, the deflection imposed by the pair of forces at the gear mesh is nil for all axial and bending displacement components while the angles of torsion in $\left\{\widehat{X}_0\right\}$ correspond to two rigid-body rotations of the pinion and the gear shafts about the axes (O_1, **z**) and (O_2, **z**), respectively. Separating the bending-axial (subscript *BA*), and torsional components (subscript TORS), one obtains

$$\left\{\widehat{X}_0\right\} = \left\{\widehat{X}_0\right\}_{\text{TORS}}, \tag{A.6}$$

$$\left\{\widehat{X}_0\right\}_{\text{BA}} = \{0\} \tag{A.7}$$

$$\left(\text{with } \{X_0\}_{\text{TORS}} \neq \left\{\widehat{X}_0\right\}_{\text{TORS}}\right).$$

Because $\{W\}$, projection vector in the expression of transmission error, deals with torsional components only, one can deduce the following properties:

$$\{W\}^{\text{T}}\left\{\widehat{X}_0\right\} = \{W\}^{\text{T}}\left\{\widehat{X}_0\right\}_{\text{TORS}}, \tag{A.8}$$

$$\{W\}^{\text{T}}\{X_0\} = \{W\}^{\text{T}}\{X_0\}_{\text{TORS}}. \tag{A.9}$$

The torsional components of $\left\{\widehat{X}_0\right\}$ being constant on the pinion and on the gear shaft (but different on each shaft), it can be observed that $\{W\}^{\text{T}}\left\{\widehat{X}_0\right\}$ is independent of the positions of the nodes of reference (or encoders) for calculating transmission error as long as one node (encoder) is on the pinion shaft and the second one on the gear shaft. Choosing the pinion node and the gear node as references and using Eq. (A.4), one finds

$$\{W\}^{\text{T}}\left\{\widehat{X}_0\right\} = \frac{1}{\cos\beta_b}\{V\}^{\text{T}}\left\{\widehat{X}_0\right\} = \frac{1}{\cos\beta_b}\{V\}^{\text{T}}\{X_0\}. \tag{A.10}$$

A.3. Expression of $C_{wv} = \{W\}^{\text{T}}\left[\bar{K}\right]^{-1}\{V\}$

Using the same approach as for C_{vv}, one obtains

$$C_{wv} = \frac{1}{F_S}\{W\}^{\text{T}}\left\{\widehat{X}_0\right\} \tag{A.11}$$

which, after applying Eq. (A.10), gives

$$C_{wv} = \frac{1}{F_S}\frac{v_{x0}}{\cos\beta_b} = \frac{1}{k_m \cos\beta_b}. \tag{A.12}$$

A.4. Expression of $v_{xs} = \{V\}^{\mathrm{T}}\{X_S\}$

From the expression of the quasi-static displacement vector $\{X_S\}$ in Eq. (32), v_{xs} is written as

$$v_{xs} = v_{x0} + \frac{C_{vv}}{C_{wv}}(\mathrm{TE}_s - w_{x0} - \mathrm{NLTE}) \tag{A.13}$$

which, after applying Eqs. (A.3) and (A.12), finally gives

$$v_{xs} = v_{x0} + \cos\beta_b(\mathrm{TE}_s - w_{x0} - \mathrm{NLTE}). \tag{A.14}$$

References

[1] R.W. Gregory, S.L. Harris, R.G. Munro, Dynamic behaviour of spur gears, *Proceedings of the Institution of Mechanical Engineers* 178 (1963) 261–266.
[2] A. Kubo, Stress condition, vibrational exciting force and contact pattern of helical gears with manufacturing and alignment errors, *American Society of Mechanical Engineers, Journal of Mechanical Design* 100 (1978) 77–84.
[3] H.N. Ozgüven, D.R. Houser, Mathematical models used in gear dynamics—a review, *Journal of Sound and Vibration* 121 (1988) 383–411.
[4] A. Kahraman, H.N. Ozgüven, D.R. Houser, J. Zakrajsek, Dynamic analysis of geared rotors by finite elements, *American Society of Mechanical Engineers, Journal of Mechanical Design* 114 (1992) 507–514.
[5] L. Vedmar, B. Henriksson, A general approach for determining dynamic forces in spur gears, *American Society of Mechanical Engineers, Journal of Mechanical Design* 120 (1998) 593–598.
[6] W.D. Mark, Analysis of the vibratory excitation of gear systems: basic theory, *Journal of the Acoustical Society of America* 63 (5) (1978) 1409–1450.
[7] R. G. Munro, Optimum profile relief and transmission error in spur gears, *Proceedings of the First Institution of Mechanical Engineers International Conference on Gearbox Noise and Vibration*, Cambridge, 1990, pp. 35–43.
[8] S. Sundaresan, K. Ishii, D.R. Houser, Design of helical gears with minimum transmission error under manufacturing and operating variances, *Proceedings of the JSME International Conference on Motion and Power Transmission, MPT 1991*, Hiroshima, November 23–26, 1991, pp. 92–97.
[9] R.W. Gregory, S.L. Harris, R.G. Munro, Torsional motion of a pair of spur gears, *Proceedings of the Institution of Mechanical Engineers* 178 (1963–64) 166–173.
[10] P. Velex, M. Maatar, A mathematical model for analyzing the influence of shape deviations and mounting errors on gear dynamic behaviour, *Journal of Sound and Vibration* 191 (5) (1996) 629–660.
[11] F. Küçükay, Dynamic behaviour of high speed gears, *Proceedings of the Third International Conference on Vibrations in Rotating Machinery, Institution of Mechanical Engineers*, York, 11–13 September 1984, pp. 81–90.
[12] P. Velex, M. Maatar, J.P. Raclot, Some numerical methods for the simulation of geared transmission dynamic behaviour—formulation and assessment, *American Society of Mechanical Engineers, Journal of Mechanical Design* 119 (3) (1997) 292–298.
[13] S.L. Harris, Dynamic loads on the teeth of spur gears, *Proceedings of the Institution of Mechanical Engineers* 172 (1958) 87–112.
[14] R.G. Munro, The DC component of gear transmission error, *Proceedings of the Fifth ASME International Power Transmission and Gearing Conference*, Chicago, 1989, pp. 467–470.
[15] P. Velex, Some problems in the modelling of gear dynamic behaviour, *Proceedings of the JSME International Conference on Motion and Power Transmission*, MPT 2001, Vol. 1, Fukuoka, November 15–17, 2001, pp. 45–50.

[16] S. Baud, P. Velex, Static and dynamic tooth loading in spur and helical geared systems—experiments and model validation, *American Society of Mechanical Engineers, Journal of Mechanical Design* 124 (2) (2002) 334–346.
[17] C. Weber, K. Banaschek, *Formänderung und Profilrücknahme bei Gerad-und Schrägverzahnten Rädern*, Heft 11, F. Vieweg und Sohn, Braunschweig, 1953, Germany, 88pp.
[18] W.J. O'Donnell, The additional deflection of a cantilever due to the elasticity of the support, *American Society of Mechanical Engineers, Journal of Applied Mechanics* 27 (1960) 461–464.
[19] H.N. Ozgüven, D.R. Houser, Dynamic analysis of high speed gears by using loaded static transmission error, *Journal of Sound and Vibration* 125 (1) (1988) 71–83.
[20] J.P. Raclot, P. Velex, Simulation of the dynamic behaviour of single and multi-stage geared systems with shape deviations and mounting errors by using a spectral method, *Journal of Sound and Vibration* 220 (5) (1999) 861–903.
[21] M. Ajmi, P. Velex, A model for simulating the quasi-static and dynamic behaviour of solid wide-faced spur and helical gears, *Mechanism and Machine Theory* 40 (2005) 173–190.
[22] H. Lipkin, J. Duffy, Sir Robert Stawell Ball and methodologies of modern screw theory, *Journal of Mechanical Engineering Science, Proceedings of the Institution of Mechanical Engineers* 216 (C1) (2002) 1–11.